Pertanika J. Sci. & Technol. 25 (2): 527 - 536 (2017)

SCIENCE & TECHNOLOGY

Journal homepage: http://www.pertanika.upm.edu.my/

Phase Transition and Dielectric Properties of $0.9Pb(Fe_{1/2}Nb_{1/2})O_3-0.1PbTiO_3$ Modified with Nano ZnO

Hassakorn Wattanasarn[1,2]*, Wattana Photankham[1,2], Peerapat Pattumma[1,2] and Rattikorn Yimnirun[3]

[1]Thermoelectrics Research Centre, Research and Development Institution, Sakon Nakhon Rajabhat University, 680 Nittayo Road, Mueang District, Sakon Nakhon, 47000 Thailand

[2]Program of Physics, Faculty of Science and Technology, Sakon Nakhon Rajabhat University, 680 Nittayo Road, Mueang District, Sakon Nakhon, 47000 Thailand

[3]School of Physics, Institute of Science, and COE−NANOTEC−SUT on Advanced Functional Nanomaterials, Suranaree University of Technology, Nakhon Ratchasima, 30000 Thailand

ABSTRACT

Samples of $0.9Pb(Fe_{1/2}Nb_{1/2})O_3-0.1PbTiO_3$ were mixed with ZnO at 0, 1, 2, and 3 wt.%, and were synthesised by mixed oxide through a two-step sintering method. Phase transition of the samples was analysed by using X–ray diffractometer (XRD) and Fourier transform infrared spectroscopy (FTIR). The dielectric properties were determined by LCR meter at 1 kHz, 10 kHz, and 100 kHz. The results showed that the morphotropic phase boundary of 0.9PFN−0.1PT shifting to tetragonal phase and suppressed pyrochlore phase when ZnO was added into 0.9PFN−0.1PT. In addition, FTIR spectra peak showed zinc and oxygen bond bonding vibration at frequencies range 3,452 cm^{-1} and 3,792 cm^{-1} after level doping ZnO of 3 wt.%. The samples exhibited the maximum dielectric constant at temperature for 144ºC. The dispersion of dielectric constantly decreased with increasing ZnO contents. The relaxor ferroelectric of 0.9PFN−0.1PT ceramic shifted to normal ferroelectric with increasing ZnO contents.

Keywords: Dielectric properties, ferroelectric material, FTIR, microstructure, XRD, ZnO

INTRODUCTION

Many applications in memories and sensors are applied from piezoelectric devices which are produced from relaxor ferroelectric ceramics with lead–based complex perovskite structure, and are favoured by researchers in physics field (Cross, 1996; Vladimír et al., 2003). $Pb(Fe_{1/2}Nb_{1/2})O_3-PbTiO_3$ (PFN−PT) ceramic is well known for ferroelectric

Article history:
Received: 13 May 2016
Accepted: 09 August 2016

E-mail addresses:
w_hussakorn@hotmail.com (Hassakorn Wattanasarn),
dagon_wat@hotmail.com (Wattana Photankham),
peerapatpongpang2522@gmail.com (Peerapat Pattumma),
rattikorn@g.sut.ac.th (Rattikorn Yimnirun)
*Corresponding Author

ISSN: 0128-7680

materials that have been developed by researchers for portable microelectronic applications (Kim et al., 2011). Generally, the perovskite structure of ferroelectrics ceramic has been obtained on the basis of complex lead niobate perovskite $Pb(B'Nb)O_3$ (where $B' = Mg^{2+}$, Zn^{2+}, Fe^{3+}) (Mackeviciute, et al., 2015). Meanwhile, the regarded pyrochlore phase exists in microstructure of PFN−PT ceramics because of Pb^{2+} vacancy. Pyrochlore phase was suppressed by either using columbite method or two-steps sintering into mixed oxide process (Moetakef & Nemati, 2007) which had an effect to produce piezoelectric properties. Singh et al. (2008) found that the structure of $(1 - x)$ PFN–xPT was in monoclinic phase for $x < 0.05$ and predominantly tetragonal phase for $x > 0.10$, whereas the two phases coexist in the intermediate composition range. The morphotropic phase boundary (MPB) depends on composition, which is a technique for showing maximum dielectric properties (Park & Shrout, 1997) $(1 - x)$PFN–xPT is a maximum peak of the dielectric constant at $x = 0.08$ (Singh et al., 2008). The $(1 - x)$ PFN–xPT system is reported on the dielectric properties of highly leaky samples (Wang et al., 2005), which cannot attain the phase transition at a higher temperature. To improve the physical and electrical properties for applications lead-based relaxor ceramics,which were produced by doping with transition oxides (ZnO, CuO, La_2O, Fe_2O, MnO_2, etc.), have been intensively investigated. For example, Zhang et al. (2009) found that Ce doped PNW–PMN– PZT ceramics were able to optimize piezoelectric and dielectric properties with stable temperature. In addition, the researchers (Kang et al., 2004; Feng, Rongzi et al., 2009) revealed that PMN−PNN−PZT ceramics modified with Zn^{2+} and Li^{+} ions exhibited excellent electrical properties and Curie temperature (T_C = 251ºC), at 960ºC for low sintering temperature. In addition, Yan et al. (2012) studied the effect of MnO_2 on the phase structure and ferroelectric behaviour of PMN–PZT ceramics found that the Mn^{2+} ion substitute on Zr^{4+} and Ti^{4+} sites induced a hardening effect. In addition, Wattanasarn and Seetawan (Wattanasarn & Seetawan, 2014) reported Zn atom has affected the tetragonal structure and improved the highest temperature that can be achieved due to a single normal vibration (Debye temperature) of $PbTiO_3$ with first principle calculation.

The synthesised ferroelectric material plays a crucial role for responding to the microstructure and electrical properties. In this work, the $0.9Pb(Fe_{1/2}Nb_{1/2})O_3$−$0.1PbTiO_3$ (0.9PFN–0.1PT) ceramics occupy into MPB of $(1 - x)$PFN–xPT system which is prepared by columbite mixed oxide. The ZnO was added into 0.9PFN−0.1PT ceramics with solid state reaction. The samples were investigated in microscale for traces of atomic vibration by Fourier transform infrared spectroscopy (FTIR) method. In the phase transition, the temperature is dependent on the dielectric behaviour that corresponded to ferroelectric properties of 0.9PFN–0.1PT and 0.9PFN−0.1PT: xZn ceramics. By adding ZnO into the 0.9PFN–0.1PT it is expected to decrease the pyrochlore phase, as well as affect the dielectric properties of 0.9PFN–0.1PT.

MATERIALS AND METHOD

The 0.9PFN–0.1PT: xZn were obtained by solid state reaction technique, limiting Zn atoms substituted in any vacancies and also protecting the temperature of maximum dielectric constant which would be shifted when ZnO contents were increased, and the researcher chose $x = 0$, 1, 2, and 3 wt.%. In this study, the 0.9PFN–0.1PT: xZn ceramics were synthesised by columbite method. Firstly, iron niobate ($Fe_2Nb_2O_4$: FN) was prepared from the stoichiometric ratio for

precursor, which composed of Fe_2O_3 (98%), and Nb_2O_5 (99.9%). The materials were mixed with ball milling, and fired at 1000ºC for 6 h. Secondly, 0.9PFN–0.1PT: *x*Zn was prepared by mixing oxide materials that were composed of FN, PbO (99%) excess with 4 mol% for compensate PbO which volatilised during the heat treatment, TiO_2 (98%) and ZnO (< 100 nm). These powders were mixed in stoichiometric ratio of the samples, and then the milling process in deionize water took 24 h and was vaporised by hotplate. The mixed powder was pressed through the following two-steps sintering process (Moetakef & Nemati, 2007). In the first step, the sample was pressed to a pellet for calcination, treated in PbO atmosphere by covering the sample with $Pb(Zr_{1-x}Ti_x)O_3$ (PZT) powder in an alumina crucible, and heated to 850ºC with the heating rate of 10°C min^{-1}. Then it was soaked at that temperature for 4 h, and then cooled down at room temperature. After that, the sample was crushed into powder and then mixed with polyvinyl alcohol solution (5 wt.%), and pressed at 320 MPa to form disc shapes with 10 mm in diameter and 1.2 mm in thickness The second step for sintering at a high temperature was for the disc sample to be maintained under lead atmosphere during the firing process. The sample pellets were embedded in the PZT powder which was derived from the previous step. The sample was then sintered at 1100ºC for 2 h with a heating rate of 10ºC min^{-1}. After that, the sintered sample was polished to remove the lead-rich layer on the surface of the sample.

The plane patterns of sintered samples were determined with an X–ray diffractometer (Shimadzu XRD−6100). The XRD patterns were recorded at room temperature with Cu Kα radiation. Diffraction intensity was measured at 2θ in range of 20º to 60º with a step up of 0.02º. The bulk density of the sample was measured using the Archimedes method in order to compare it with theoretical density. The FTIR absorption in the spectral range 400−4,000 cm^{-1} was obtained. The IR absorption measurements were done using the KBr pellet technique. The samples were crushed in an agate mortar to obtain particles. This procedure was applied every time to fragments of a sample to avoid structural modifications due to ambient moisture. The samples were coated with silver paint on the sample surfaces as electrode for dielectric measurements. The capacitances were obtained using Chen Hwa 1061 LCR–Meter connected to the sample electrode in a chamber that was heated at a temperature from 30–300ºC. In this study, the dielectric constants were measured at a discrete frequency range of 1 kHz to 100 kHz. The capacitances were used to investigate the dielectric constants from $\varepsilon_r = Ct / \varepsilon_0 A$; where C is the capacitance of the sample, t and A are the thickness and the area of the electrode, respectively, and ε_0 is the dielectric permittivity in vacuum.

RESULTS AND DISCUSSION

The XRD technique was run on CuKa (wavelength 1.54056 Å) for investigated phase patterns of 0.9PFN–0.1PT: *x*Zn (*x* = 0, 1, 2, and 3 wt.%) as shown in Figure 1. The samples were identified to the characteristic patterns of complex perovskite structure ($A(B'B'')O_3$). Usually, 0.9PFN–0.1PT exhibits morphotropic phase boundary (MPB) and then gradually shifts to tetragonal phase with increasing PT contents (Ciomega, et al., 2013). In Figure 1, the ZnO content doped into 0.9PFN–0.1PT. It observed that pyrochlore phase was suppressed with increasing ZnO contents as presented in Figure 1 (inset). The phase transformation from

the MPB phase eventually shifted to tetragonal phase with increasing ZnO contents. Using 2θ data from 20º to 60º of the XRD results evaluated the percentage of perovskite structure, lattice parameters a, c, tetragonality (c/a), bulk density and relative density are listed in Table 1. This result implied that not only Zn^{2+} ion can be a reducing Pb^{2+} vacancy but it also increases tetragonality of 0.9PFN–0.1PT. Furthermore, Peak of 0.9PFN–0.1PT is shifted due to substitution in B site in perovskite structure and deflect structure, which Zn^{2+} (ionic radii 0.8 Å) substituted Fe^{3+}(0.75 Å) and Nb (0.86 Å), lead to compressing lattice strain in microstructure and effect to shifted peak (Zhang, et al., 2016).

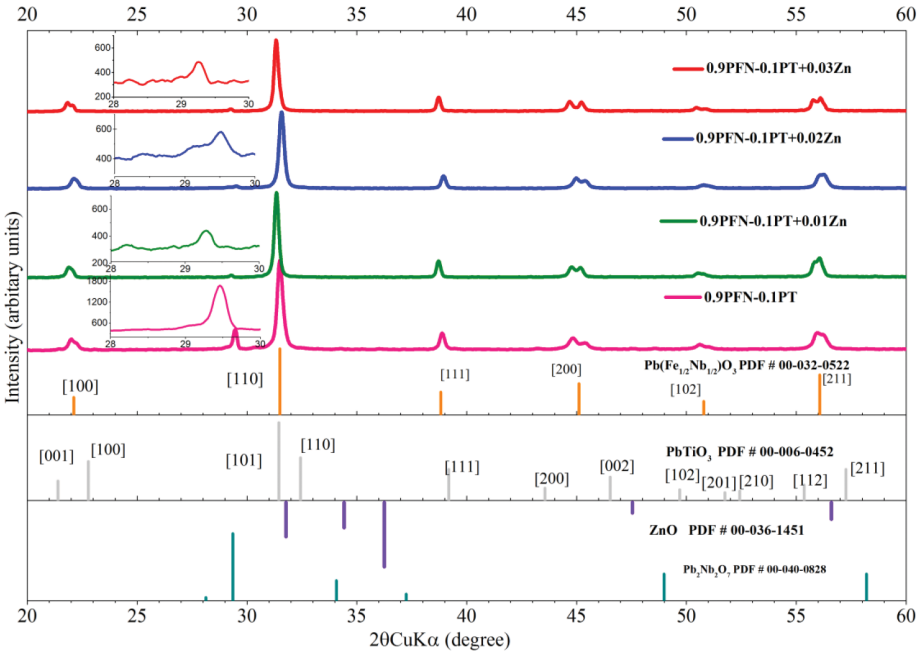

Figure 1. The illustrated of XRD patterns of 0.9PFN−0.1PT: *x*Zn (*x* = 0, 1, 2, and 3 wt.%) ceramics

Table 1

Lattice parameters a and c, tetragonality (c/a), Rietveld refinement using data from 20º to 60º of the XRD results in Figure 1. Experiment Density (g cm^{-3}), and relative density (%)

0.9PFN–0.1PT: *x*Zn	% Perovskite	a (Å)	c (Å)	c/a	Experiment Density	Relative density
x = 0	80.11	0.4008	0.4063	1.013	7.701	92.57
x = 1	91.61	0.3986	0.4023	1.009	7.687	89.55
x = 2	92.28	0.3987	0.4021	1.008	7.764	90.59
x = 3	92.36	0.3975	0.4019	1.011	7.567	87.87

The (200) plane is a single peak for the cubic, while (200)T and (002)T plane can be found in tetragonal phase (Kang, et al., 2004). It is noted that the broad peak exhibited the tetragonal phase split into two peaks at (200) plane. The major differences of XRD pattern are analysed on the peaks of (200) plane which ranged from 44º−46º. In order to determine the phase transition of various samples accurately, the broad peak of (002) plane lines of three samples were obtained by extracting from XRD pattern range 44º−46º, as presented in Figure 2. The (200) reflections splits to (200)T and (002)T were found by fitting Gaussian peaks (red and green lines). The MPB phase for $x = 0$. The coexistence of equal quantities of the MPB region, in the tetragonal and cubic phases is well known (Feng et al., 2009; Yan et al., 2012). Consequently, X-ray diffractometer is the evidence clearly of splitting on plane (200)T as shown in Figure 2. In addition, lattice parameters and tetragonality (c/a) are the reasons that justify the shift of MPB phase to tetragonal phase, that increased tetragonality (c/a) with increasing ZnO contents as listed in Table 1.

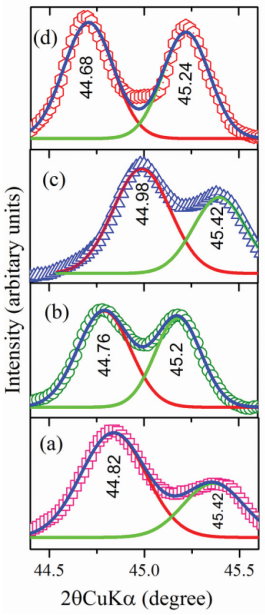

Figure 2. The phase transition of MPB to tetragonal phase on plane (200)T and (002)T (2θ = 44º−46º) of 0.9PFN–0.1PT: *x*Zn, (a) $x = 0$ wt.%, (b) $x = 1$ wt.%, (c) $x = 2$ wt.%, and (d) $x = 3$ wt.%

In order to study the vibrational properties of ZnO the sample was doped into 0.9PFN–0.1PT. Fourier transform infrared spectroscopy (FTIR) spectra were in the region of 400–4,000 cm^{-1} at room temperature, as depicted in Figure 3. It observed that all samples exhibited quite similarly to peaks confirming 0.9PFN−0.1PT: *x*Zn. Absorption bands was around 605 cm^{-1} for all samples which attributed to O–Ti–O and Nb–O bending vibrations of TiO_6 and NbO_6 octahedral groups respectively (Eastel & Udy, 1972; Shimizu et al., 1977). Furthermore, FTIR peak showed intensity of Zn at 3,412 cm^{-1} and 3,792 cm^{-1} for 2 wt.% and 3 wt.%. In contrast, 0.9PFN–0.1PT: 1Zn removed any peak on this range due to the complexity of zinc with the

substitution in complex perovskite structure (Kwon et al., 2002; Silva & Zaniquelli, 2002; Paterson, et. al, 2015). In addition, FTIR peaks shifted due to some structural modifications that occurred during the dioxygen intercalation process (Laureano, et al., 1998). It is noted that Zn atom has affected the ferroelectric materials that is phase transition corresponding with XRD data.

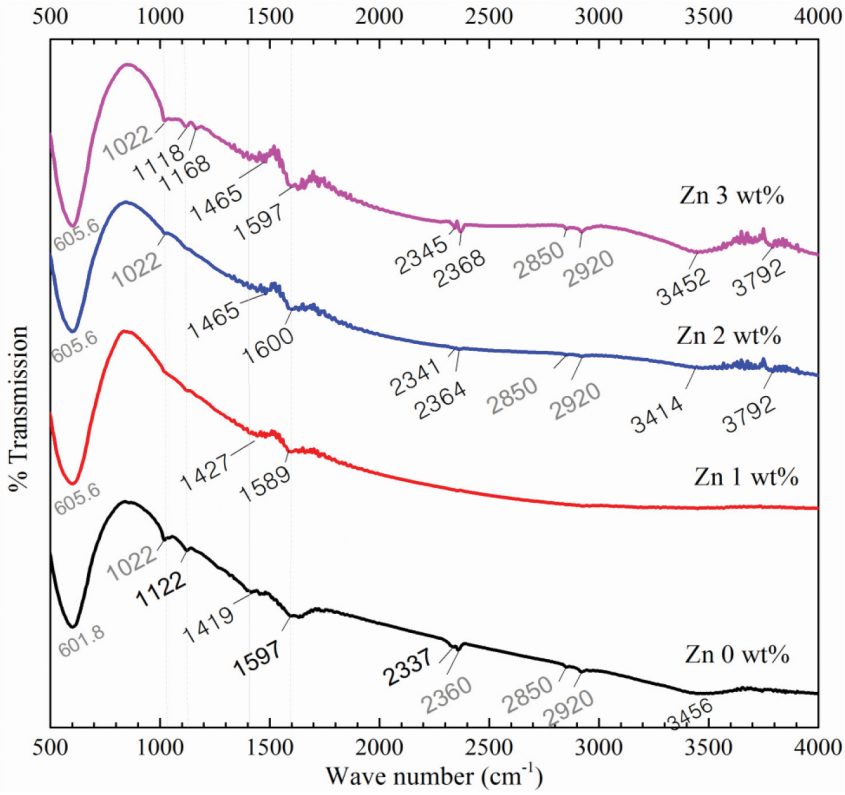

Figure 3. Fourier transform infrared spectra (FTIR) of 0.9PFN−0.1PT: *x*Zn (*x* = 0, 1, 2, and 3 wt.%) ceramics

Generally, dielectric behaviour is favoured to explain the existence in microscopic and nanoscopic scales. Dielectric constant (ε_r) and dielectric loss ($\tan\delta$) as a function of temperature at various frequencies of 0.9PFN–0.1PT: *x*Zn was found to have the maximum dielectric constant at temperature 144°C, as shown in Figure 4. The ε_r of 0.9PFN–0.1PT was found to be very high at 1 kHz see in Figure 4(a) (inset), and then rapidly decreasing. The broad wide peaks of dielectric dispersion appeared with increasing frequency, as shown in Figure 4(a). Similarly, 0.9PFN−0.1PT: 1Zn exhibited broad wide peaks of dielectric dispersion and increased when the temperature was higher than 150ºC is depicted in Figure 4(b). It is evident that 0.9PFN−0.1PT exhibited a diffuse ferroelectric phase transition with a transition temperature that caused B site ions disorder in complex perovskite. Figure 4(c) and Figure 4(d) showed a ferroelectric behaviour of 0.9PFN−0.1PT:2Zn, and 0.9PFN−0.1PT:3Zn respectively,

with a broad wide peak transformed to sharp peak and dielectric constant, which was observed to significantly decrease when ZnO was added. It was assumed that the spontaneous polarization (domain wall) dynamically changed the polar nanoregions' direction at the above average transition temperature (Mackeviciute, et al., 2015). It exhibited that increasing ZnO content into 0.9PFN−0.1PT would be affected to relaxor ferroelectric behaviours that were ordered structure of a short range of heterogeneous in mixed oxide powder.

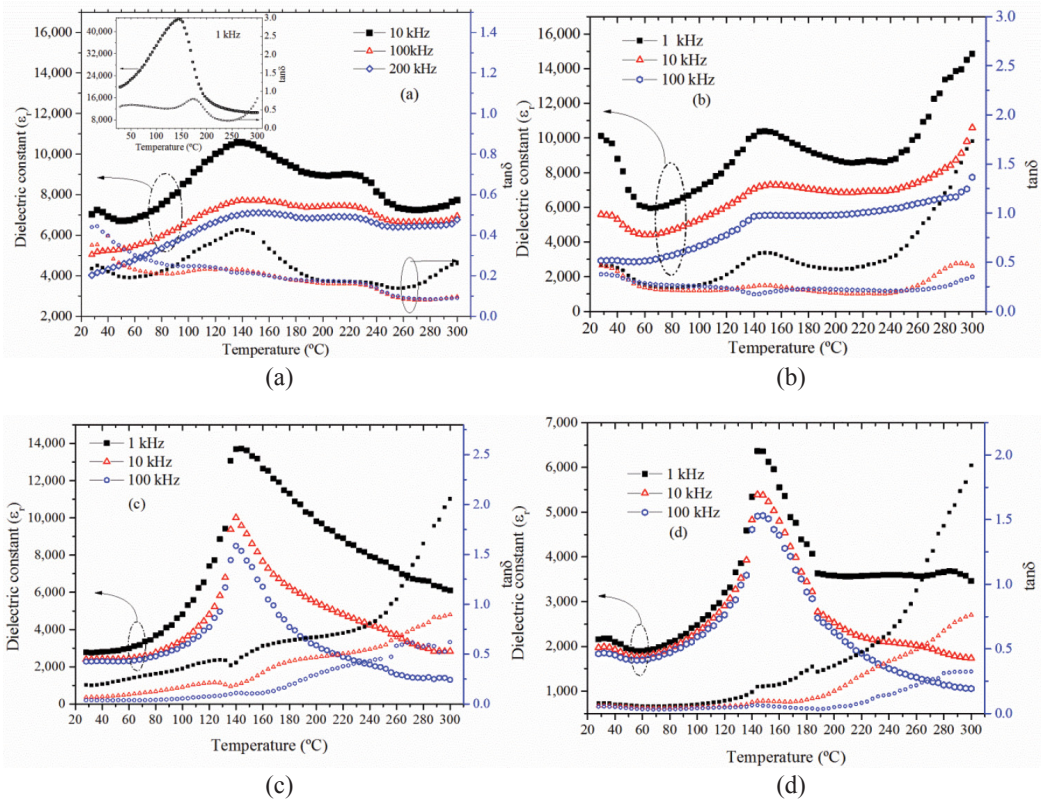

Figure 4. Illustrating the temperature and frequency dependence of dielectric constant and dielectric losses of 0.9PFN−0.1PT: *x*Zn; (a) *x* = 0 wt.%; (b) *x* = 1 wt.%; (c) *x* = 2 wt.%; and (d) *x* = 3 wt.%

The dielectric loss ($\tan\delta$) of 0.9PFN−0.1PT: *x*Zn (*x* = 0, 1, 2, and 3 wt.%) ceramics are illustrated in Figure 4(a)–(e), the $\tan\delta$ shows dependence with frequencies of 0.9PFN–0.1PT: *x*Zn at different temperatures. It was found that $\tan\delta$ rose with increasing temperatures, as well as the $\tan\delta$ decreased with increasing frequency of the applied alternative current. This may be due to the hopping of electron that cannot follow the frequencies of applied current. Moreover, the dispersion in $\tan\delta$ at higher temperatures was observed for the samples. This is attributed to the conductivity of the ceramics. In addition, the oxygen vacancies and PbO evaporated during higher temperature sintering. Besides, appearing peak of $\tan\delta$ is suggested that long range order in relaxor ferroelectric phase affected by heating (Ni, Luo, Pan, Zhang, & Chen, 2012).

CONCLUSION

Modified ZnO into 0.9PFN−0.1PT: *x*Zn (*x* = 0, 1, 2, and 3 wt.%) ceramics were prepared by the two-step sintering process. The phase transition was demonstrated by using X–ray diffraction technique. The structures of the 0.9PFN−0.1PT experienced a gradual transition process from MPB phase to tetragonal phase with ZnO contents added. FTIR peak showed transmission of bonding vibration of Zn at 3,412 cm^{-1} and 3,792 cm^{-1} for 2 wt.% and 3 wt.%, 0.9PFN−0.1PT: 1Zn disappeared at any peak on these ranges due to homogeneous substitution of zinc atom into complex perovskite structure. 0.9PFN–0.1PT: *x*Zn exhibited the maximum dielectric constant at a temperature of 144ºC, the broad wide peak of dielectric constant was transformed to sharp peak and dielectric constant significantly decreased by adding ZnO. The dielectric loss increased at higher temperatures, as well as decreased with increasing frequency of the applied alternative current. These results confirmed the effect of ZnO to micro-scale and nano-scale transition into 0.9PFN−0.1PT. These results can also be attributed to ferroelectric and relaxor ferroelectric behaviour, and will be useful for electronic applications.

ACKNOWLEDGEMENTS

We would like thank the Research and Development Institute of Rajabhat Sakon Nakhon for the financial support given to us to conduct this research. We would also acknowledge the Science and Technology Department of Rajabhat Sakon Nakhon for FTIR. In addition, we are thankful to Sakon Nakhon Rajabhat University International Conference 2015 (SNRU-IC 2015) team for preparing the documents and for commenting and improving the English language presentation of this paper.

REFERENCES

Ciomega, C. E., Neagu, A. M., Pop, M. V., Airimioaei, M., Tascu, S., Schileo, G., & Mitoseriu, L. (2013). Ferroelectric and dielectric properties of ferrite–ferroelectric ceramic composites. *Journal of Applied Physics*, *113*, 074103_1-074103_4.

Cross, L. E. (1996). Ferroelectric materials for electromechanical transducer applications. *Materials chemistry and physics, 43*(2), 108-115.

Eastel, A. J., & Udy, D. J. (1972). Preparation and properties of potassium titanes. *High Temperature Science*, *4*(6), 487-495.

Feng, G., Rongzi, H., Jiaji, L., Zhen, L., & Chang, S. T. (2009). Effects of ZnO/ Li_2O co doping on micro structure and piezoelectric properties of low-temperature sintered PMN–PNN–PZT ceramics. *Ceramics International*, *35*(5), 1863-1869.

Gao, Y., Xu, H. Y., Wu, He, T., Xu, G., & Luo, H. (2001). Growth and Dielectric Properties of 0.48 $Pb(Fe_{1/2}Nb_{1/2})O_3$–0.52 $PbTiO_3$ Single Crystal. *Japanese Journal of Applied Physic*, *40*(8R), 4998-4999.

Kang, S. H., Lee, D. S., Lee, S. Y., Kim, I. W., Kim, J. S., Park, E. C., & Lee, J. S. (2004). Pyroelectric and piezoelectric properties of yttrium-doped 0.15$[Pb(Ni_{1/3}Nb_{2/3})O_3]$–0.85$[Pb(Zr_{1/2}Ti_{1/2})O_3]$ ceramics. *Ceramics International*, *30*(7), 1453-1457.

Kim, H. S., Kim, J. H., & Kim, J. (2011). A Review of Piezoelectric Energy Harvesting Based on Vibration. *International Journal of Precision Engineering and Manufacturing*, *12*(6), 1129-1141.

Kwon, Y. J., Kim, K. H., Lim, C. S., & Shim, K. B. (2002). Characterization of ZnO nanopowders synthesized by the polymerized complex method via an organo chemical route. *Journal of Ceramic Processing Research*, *3*, 146–149.

Laureano, M. R., Enrique, R. L., Miguel, A. G., Marıa, M. L., Bruque, S., & Gabas, M. (1998). A Peroxoniobium Phosphate Derived from $NbOPO_4$ $-3H_2O$. *Journal of Solid State Chemistry*, *137*(2), 289-294.

Mackeviciute, R., Goian, V., Greicius, S., Grigalaitis, R., Nuzhnyy, D., Hol, J., & Banys, J. (2015). Lattice dynamics and broad-band dielectric properties of multiferroic $Pb(Fe_{1/2}Nb_{1/2})O_3$ ceramics. *Journal of Applied Physics*, *117*(8), 084101.

Moetakef, P., & Nemati, Z. A. (2007). Synthesis of PMN pyrochlore free ceramics via a modified mixed oxide method. *Journal of Electroceramics*, *19*(2-3), 207-213.

Ni, F., Luo, L. H., Pan, X. Y., Zhang, Y. P., & Chen, H. B. (2012). Piezoelectric and dielectric properties of $Bi_{0.5}Na_{0.5}TiO_3$− $Bi_{0.5}K_{0.5}TiO_3$−$Ba_{0.77}Ca_{0.23}TiO_3$ lead–free piezoelectric ceramics. *Journal of Materials Science*, *47*(7), 3354–3360.

Park, S. E., & Shrout, T. R. (1997). Ultrahigh strain and piezoelectric behavior in relaxor based ferroelectric single crystals. *Applied Physics Letters*, *82*(4), 1804-1811.

Paterson, A., Wong, H. T., Liu, Z., Ren, W., & Ye, Z. G. (2015). Synthesis, structure and electric properties of a new lead-free ferroelectric solid solution of $(1-x)BaTiO_3$–$xBi(Zn_{2/3}Nb_{1/3})O_3$. *Ceramics International*, *41*, S57–S62.

Shimizu, T., Morita, T., Yanagida, H., & Hashimoto, K. (1977). Crystallographic Study of Potassium Hexa–titanate. *Journal of the Ceramic Association Japan*, *85*(980), 189-193.

Silva, R. F., & Zaniquelli, M. E. (2002). Morphology of nanometric size particulate aluminium doped zinc oxide films. *Colloids and Surfaces A: Physicochemical and Engineering Aspects*, *198–200*, 551–558.

Singh, S., Pandey, D., Yoon, S., Baik, S., & Shin, N. (2008). Resolving the characteristics of morphotropic phase boundary in the $(1-x)Pb(Fe_{1/2}Nb_{1/2})O_3$–$xPbTiO_3$ system: a combined dielectric and synchrotron x-ray diffraction study. *Applied Physics Letter*, *93*(18), 182910_1-182910_3.

Vladimír, K. A., Carlos, Jaroslav, B., Helena, B., & Karol, S. (2003). Effect of PMN modification on structure and electrical response of xPMN–(1−x)PZT ceramic systems. *Journal of the European Ceramic Society*, *23*(7), 1157-1166.

Wang, J., Tang, X., Chan, H. L., & Choy, C. L. (2005). Dielectric relaxation and electrical properties of 0.94Pb(Fe 1/2Nb1/2)O3− $0.06PbTiO_3$ single crystals. *Applied Physics Letters*, *86*(15), 152907_1–152907_3.

Wattanasarn, H., & Seetawan, T. (2014). Elastic Properties and Debye Temperature of Zn Doped $PbTiO_3$ from First Principles Calculation. *Integrated Ferroelectrics*, *155*(1), 59-65.

Yan, Y. K., Correa, M., Cho, K. H., Katiyar, R. S., & Priya, S. (2012). Phase transition and temperature stability of piezoelectric properties in Mn modified $Pb(Mg_{1/3}Nb_{2/3})O_3$–$PbZrO_3$–$PbTiO_3$ ceramics. *Applied Physics Letters*, *100*(15), 152902_1-152902_3.

Zhang, C. H., Chi, Q., He, X., Lin, J. Q., Chen, Y., Liu, L. Z., & Lei (2016). Microstructure and electric properties of Nb doping $x(Ba_{0.7}Ca_{0.3})TiO_3$-$(1-x)Ba(Zr_{0.2}Ti_{0.8})O_3$ ceramics. *Journal of Alloys and Compounds*, *685*, 936-940.

Zhang, R., Yang, Z., Chao, X., & Kang, C. (2009). Effects of CeO_2 addition on the piezoelectric properties of PNW–PMN–PZT ceramics. *Ceramics International*, *35*(1), 199-204.